# Modeling the oxidation kinetics of titanium alloys: Review, method and application to Ti-64 and Ti-6242s alloys

Nicolas Vaché, Yannick Cadoret, Ben Dod, Daniel Monceau

# Modeling the oxidation kinetics of titanium alloys: Review, method and application to Ti-64 and Ti-6242s alloys

N. Vaché [a], Y. Cadoret [b], B. Dod [b], D. Monceau [a,*]

[a] CIRIMAT, Université de Toulouse, CNRS, INP-ENSIACET, 4 allée Emile Monso, 31030 Toulouse, France
[b] Airbus Operations SAS, 316 Route de Bayonne, 31060, Toulouse, France

ARTICLE INFO

*Keywords:*
Titanium
Modeling studies
Oxidation
Oxygen affected zone
Embrittlement
Oxide scale

ABSTRACT

The oxidation kinetics of Ti-6Al-4V and Ti-6Al-2Sn-4Zr-2Mo-Si were reviewed in the range 450−650 °C. A method to fit these data was conceived and applied to these alloys, allowing the prediction of mass gain, oxygen diffusion coefficient, embrittlement depth and oxide scale thickness. Prediction diagrams are produced and discussed through the prism of aeronautical applications; discrepancies between modeled and experimental data are discussed. This paper shows that despite Ti-6Al-4V experienced larger mass gains than Ti-6Al-2Sn-4Zr-2Mo-Si, the two alloys have an equivalent behavior in terms of oxygen dissolution and diffusion, over a wide range of exposure durations.

## 1. Introduction

Every second, 6 kg of titanium are produced worldwide [1]. The main advantage of using titanium alloys remains their very good mechanical properties given their low density. This is why more and more technical sectors, from biomedical to automotive industries and especially aircraft manufacturing, are using them. Beyond their very interesting specific mechanical properties, titanium alloys have been progressively improved to fulfill a demand for high temperature applications in aircraft engine parts or at the outlet of gas turbines. The durability of titanium alloys exposed to temperature has been studied since the end of the 1960s and space exploration.

In 1970 a study on the oxidation and embrittlement of the Ti-6Al-2Sn-4Zr-2Mo alloy (Ti-6242 or Ti-6242s for its improved version alloyed with silicon) was carried out by Shamblen and Redden from the National Aeronautics and Space Administration (NASA) [2]. Nowadays, this alloy is still used and recent publications continue to investigate its oxidation behavior [3–6]. The oxidation behavior of a titanium alloy can essentially be described as the sum of two phenomena: the formation of an outer layer of titanium dioxide $TiO_2$ which may include alumina precipitates, and the interstitial diffusion of oxygen in the metallic matrix. The diffusion of oxygen is made all the easier because, like its zirconium neighbor in the periodic table, titanium in its stable hexagonal form has an oxygen solubility limit of 33 at. % over a wide range of temperatures [7]. For the body-centered cubic phase beta, the oxygen solubility limit decreases from 8 at. % at 1720 °C to about 0 at. % at 882 °C, the beta transus temperature. In commercial alloys, the beta phase is stabilized under the beta transus temperature by chemical elements, and 5 vol. % to 20 vol. % of beta phase is generally observed in TA6V and Ti-6242s alloys under 800 °C [8]. In the case of a quasi-alpha or alpha-beta alloy, the oxygen content in the beta phase corresponds to the oxygen content initially present in the phase since liquid metal elaboration. Under the beta-transus temperature, this oxygen content decreases down to a value much lower than in the alpha phase and tends towards an equilibrium value at lower temperatures.

The diffusion of oxygen in the matrix greatly influences the mechanical properties of titanium alloys, and especially decreases ductility and fatigue life. This is generally referred to as oxygen embrittlement [4,7,9–11]. Experimentally, it has been shown that for Ti-6242s and Ti-64 the thickness of the oxygen affected zone (OAZ) is much greater than that of the oxide layer; this trend decreases with increasing temperatures [12–14]. In addition, it is necessary to specify that the total weight gain, the thickness of oxide layer and the depth of the OAZ are not directly proportionate and vary depending on the studied alloy. It thus seems necessary to accurately characterize the oxygen affected zone and model its evolution in order to properly size the parts that are subjected to high temperatures for very long periods of time.

* Corresponding author.
*E-mail address:* Daniel.monceau@toulouse-inp.fr (D. Monceau).

https://doi.org/10.1016/j.corsci.2020.109041

### 1.1. Method to evaluate and model the OAZ

In practice, the thickness of the oxygen affected zone is evaluated through micrographic examination and/or hardness testing according to EN 2003-009. The measurement of the "white area" by optical metallography after a chemical etching with Kroll reagent is the most commonly used method [3,4,12,15–21]. This measurement method is easy to use and allows for the characterization of diffusion layers that are thicker than a few micrometers after a careful surface preparation protocol. However, the determination of the OAZ/matrix boundary is operator-dependent because it is carried out visually and because there can be variations in the composition of the etching solution and in the immersion or swabbing protocols. The second method consists in analyzing microhardness (Vickers, Knoop and even nanoindentation) or oxygen concentration profiles (EPMA, EDS, SIMS, XPS). Oxygen concentration profiles are often represented with a standardized concentration scale for EPMA and EDS, which means their use is limited. This representation selection is likely explained by the difficulties to accurately correct the profiles due to surface pollution. Indeed, the presence of a native oxide typically increases EDS or EPMA measurements by a value of 3–4 wt. % [22]. These techniques are treated together here because the method remains the same: it consists in determining graphically the distance at which the microhardness (or oxygen concentration) of the enriched area becomes close to that of the bulk. Based on EN 2003-009, the diffusion zone or "white layer" can be defined as the distance between the surface and the depth at which the hardness is equal to the initial hardness of the material plus 50 HV.

Kofstad and Hauffe showed that the overall oxidation kinetics of pure titanium changes with temperature (and time): from a cubic to a parabolic regime (between 350 and 650 °C for long expositions) and then to a linear regime [23]. The diffusion zone kinetics however, is described in most studies as parabolic, with a parabolic constant or a diffusion coefficient that vary according to an Arrhenius law [12,13,24,25]. The analytical modeling of oxygen diffusion and oxide scale formation in alpha titanium as well as the total mass gain in near-alpha titanium alloys have already been carried out by Kitashima et al. using a finite volume method and a principal component analysis respectively [26, 27]. A more complete numerical model, recently proposed by Ciszak et al. [28], calculates the oxygen fluxes in the oxide scale and in the metal while taking into account the displacement of the oxide/metal interface.

So far, however, no empirical modeling method based on the compilation of experimental data from the literature has been proposed to account for all oxidation aspects of Ti-64 ad Ti-6242s. This is the objective of the present paper.

## 2. A method for modeling oxidation kinetics

The main objective of this model is to be able to predict the diffusion of oxygen in the matrix and the formation of the oxygen affected zone (OAZ) and of the brittle layer during air oxidation of titanium alloys as a function of temperature and exposure time. As the establishment of this model is based on a compilation of experimental data from the literature, equations predicting the total mass gain and the formation of the oxide scale are also proposed. Once modeled, these four quantities would allow the complete behavior of a titanium alloy during high temperature oxidation to be predicted.

The model and the equations that follow have been developed assuming hypotheses that need to be detailed:

H1 - The system is considered to be semi-infinite: the diffusion zone is small compared to the size of the system

H2 - The apparent oxygen diffusion coefficient in the metallic matrix and in the oxide are constant over the concentration range studied. They can be considered as apparent and homogenized diffusion coefficients, for a given composition and microstructure.

H3 - The aforementioned diffusion coefficients follow the Arrhenius law.

H4 - The oxygen concentration at the oxide/metal interface is considered constant because it is fixed by the thermodynamic equilibrium.

H5 - The displacement of the metal/oxide interface is negligible compared to the depth of the OAZ. However, when gathering experimental data to build the model (diffusion depth measurements or OAZs), it is important to keep in mind that the oxide layer grows at the expense of the metallic matrix.

H6 - The variation in alloy density due to the presence of interstitial oxygen is considered negligible.

H7 - There is an alloy-specific oxygen concentration value, referred to as $C_{OAZ}$, which corresponds to the oxygen concentration at end of the OAZ, i.e. at the interface between the “white layer” and the bulk alloy.

H8 - There is an alloy-specific oxygen concentration value, referred to as $C_{Brittle}$, which corresponds to the oxygen concentration at the ductile-to-brittle transition.

H9 - The oxide layer is dense and shows small deviations from stoichiometry.

H10 - The potential effect of alloy microstructure was not taken into account in this model.

Some of these hypotheses are discussed and justified hereunder.

### 2.1. Diffusion of oxygen in the metal

Since the diffusion of oxygen in titanium alloys follows parabolic kinetics, and assuming a constant concentration at the surface and a constant diffusion coefficient over the concentration range studied, diffusion profiles can be modeled using the solution of Fick’s second law [29] for a semi-infinite sample (hypotheses H1, H2, H4,H5) as:

$$\frac{C_x - C_0}{C_s - C_0} = 1 - erf\left[\frac{x}{2\sqrt{Dt}}\right] \quad (1)$$

Or,

$$C_x = \left(1 - erf\left[\frac{x}{2\sqrt{Dt}}\right]\right) * (C_s - C_0) + C_0 \quad (1\ \prime)$$

where $C_0$ represents the initial concentration of the species in the metal [$C_0 = C$ (x, t = 0)], $C_S$ the surface concentration [$C_S = C$ (z = 0, t)], $D$ the apparent oxygen diffusion coefficient in the alloy and $erf$(x) the error function. Oxygen diffusion coefficients were obtained from a literature review, from the analysis of EPMA profiles using Eqs. (1) or (1′) and from microhardness profiles using the modified error function Eqs. (2) or (2′) described in [22]:

$$\frac{HV_x - HV_0}{HV_s - HV_0} = \sqrt{1 - erf\left[\frac{x}{2\sqrt{Dt}}\right]} \quad (2)$$

Or,

$$HV_x = \left[\sqrt{1 - erf\left[\frac{x}{2\sqrt{Dt}}\right]} * (HV_s - HV_0)\right] + HV_0 \quad (2\ \prime)$$

The diffusion of oxygen interstitials being a thermally activated process, the apparent diffusion coefficient can be written according to the Arrhenius law (3) with $D_O^0$ the pre-exponential factor and $Q_{diss}$ the activation energy of the apparent diffusion of oxygen into the titanium matrix (H2 and H3).

$$D = D_O^0 * \exp\left(\frac{-Q_{diss}}{RT}\right) \quad (3)$$

These two coefficients can be obtained by representing ln(D) as a function of 1/T, the constant of the linear regression is equal to $ln(D_O^0)$ and the slope to $-Q_{diff}/R$ (R is the gas constant = 8.314 J.mol$^{-1}$. K$^{-1}$).

Knowing or setting the initial oxygen concentration in the alloy and the oxygen concentration at the oxide/metal interface (H4), $C_o$ and $C_s$

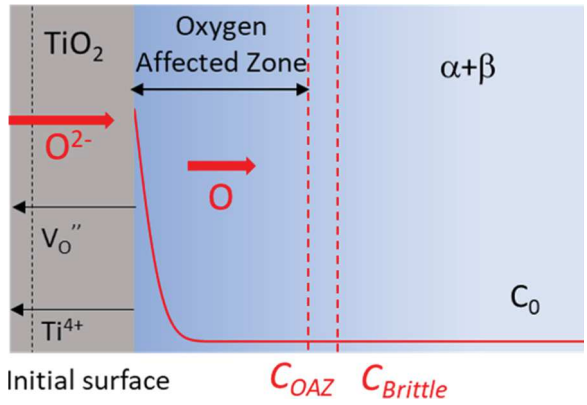


**Fig. 1.** Schematics of the oxidation of a titanium alloy.

respectively, the oxygen profile within the matrix can be plotted for any temperature and duration (within the validity range of the model) using Eqs. (1′) and (3). The mass gain due to the dissolution of oxygen in the metallic matrix, ($\frac{\Delta m}{S}_{diss}$), can then be expressed using the area under the oxygen concentration profile. By plotting the concentration as the atomic fraction of oxygen in the titanium alloy, the area under the curve is expressed in units of distance, i.e. in μm or in cm for a more convenient use. Since the variation in alloy density resulting from the presence of interstitial oxygen is considered negligible (H6), the mass gain due to oxygen dissolution, expressed in mg. cm$^{-2}$, is given by Eq. (4):

$$\frac{\Delta m}{S}_{diss} = \int_{x=0}^{x=\infty} (C - C_0)\, dx * \frac{\rho_{Ti-alloy}}{M_{Ti-alloy}} * M_{oxygen} \tag{4}$$

Where $\rho_{Ti-alloy}$ is the density of the titanium alloy (in g. cm$^{-3}$) and $M_{Ti-alloy}$ and $M_{oxygen}$ are the molar masses of the titanium alloy and oxygen (in g. mol$^{-1}$) respectively.

The mass gain by dissolution of oxygen in the matrix calculated using Eq. (4) will later be subtracted from the value of the total mass gain in order to propose an equation that models the thickness of the oxide scale formed as a function of time and temperature.

### 2.2. Modeling of Oxygen Affected Zone (OAZ) and brittle layer thicknesses

Being able to predict the oxygen concentration profile of a titanium alloy as a function of time and temperature, (using Eq. (1′)) allows the depth of the oxygen affected zone $x_{OAZ}$, to be calculated. This depth, observed as the "white layer" after chemical etching, corresponds to the distance at which the oxygen concentration reaches $C_{OAZ}$, the target concentration value (Fig. 1):

$$x_{OAZ} = \left[erf^{-1}\left(1 - \frac{C_{OAZ} - C_0}{C_s - C_0}\right)\right] * 2\sqrt{D_0 * \exp\left(\frac{-Q_{diss}}{RT}\right) * t} \tag{5}$$

Or,

$$x_{OAZ} = A * 2\sqrt{D_0 * \exp\left(\frac{-Q_{diss}}{RT}\right) * t} \tag{6}$$

With A= $erf^{-1}\left(1 - \frac{C_{OAZ}-C_0}{C_s-C_0}\right)$, the full expression of the constant A is detailed in Appendix A.

Throughout the rest of this study, the parameter $t$ will be expressed in seconds (s) and the temperature $T$ in kelvin (K).

Thus, the only remaining unknown is the oxygen concentration $C_{OAZ}$ which has never been identified experimentally, in any titanium alloy whatsoever. In order for the model to be as correct as possible, $C_{OAZ}$ was determined by fitting Eq. (5) to a dataset obtained from compiled experimental "white layer" measurements available in the literature.

From Eq. (5) it is obvious that for a similar dataset of experimental OAZ thickness measurements, the value of the oxygen concentration $C_{OAZ}$ would depend on thermokinetics coefficients $D_O^0$ and $Q_{diss}$. It can be suggested that the more available the data on diffusion coefficients and experimental OAZ thicknesses will be, the closer the determined $C_{OAZ}$ concentration will be in relation to the hypothetical oxygen concentration (H7) at the end of the "white layer".

This approach, and not a simple adjustment of the oxygen affected zone (OAZ) depths to obtain a parabolic constant $k_p$, is an astute means to propose an oxygen concentration value that is experimentally related to the end of the "white layer". The second advantage of such a model is that it can be adapted for determining another quantity associated with the diffusion of oxygen in titanium alloys, like the thickness of the brittle layer. This quantity can be found experimentally by measuring the depth of cracks that are periodically visible at the surface of an oxidized tensile test specimen [2,9,10,30].

In the case of the brittle layer depth, the same formulation as Eq. (6) can be proposed considering a ductile-to-brittle oxygen concentration $C_{brittle}$ (hypothesis H8):

$$x_{brittle} = B * 2\sqrt{D_0 * \exp\left(\frac{-Q_{diss}}{RT}\right) * t} \tag{7}$$

With B= $erf^{-1}\left(1 - \frac{C_{Brittle}-C_0}{C_s-C_0}\right)$, the full expression of the constant B is detailed in Appendix A

Values of oxygen concentration leading to a ductile-to-brittle transition can be found in the literature. Indeed, in their review of the effect of oxygen on room temperature ductility in titanium alloys, Yan et al. shows that a drop of ductility occurs in Ti-64 when the oxygen content exceeds 1 at. % (0.35 wt. %) [31]. For Ti-6242s, Shenoy et al. determined a ductile-to-brittle oxygen content of 0.5 at. % from the conversion of the ductile-to-brittle microhardness criterion of Shamblen & Redden (ΔHV = 40) [24]. However, experimental data concerning brittle layers formed on oxidized titanium samples after tensile test remains scarce. This makes it impossible to validate Eq. (7) with the two concentrations proposed above, or to determine $C_{Brittle}$ by adjusting the data as done with $C_{OAZ}$.

### 2.3. Modeling total mass gain and oxide scale thickness

In the model proposed in this paper, the total mass gain and the mass gain due to the formation of the oxide scale are linked by the mass balance Eq. (8) with the mass gain due to oxygen dissolution in the metal already calculated independently using Eqs. (1′) and (4). Assuming that the diffusion of oxygen in the matrix and the formation of the oxide layer both follow parabolic kinetics with the parabolic constants $k_{p\ diss}$ and $k_{p\ oxide}$ for mass gain due to dissolution of oxygen into the metal and the oxide growth respectively, it can be shown that the evolution of the total mass also follows parabolic kinetics (9). This last equation also highlights the fact that the parabolic constants cannot be added whereas the square roots of $k_{p\ diss}$ and $k_{p\ oxide}$, are (10). With parabolic constants following Arrhenius laws (H3), the activation energy of the total mass gain $Q_{tot}$ is a complex combination of the activation energies $Q_{diss}$ and $Q_{oxide}$ and pre-exponential factor $k^0_{p\ tot}$, $k^0_{p\ diss}$ and $k^0_{p\ oxide}$ (11).

$$\frac{\Delta m}{S}_{tot} = \frac{\Delta m}{S}_{diss} + \frac{\Delta m}{S}_{oxide} \tag{8}$$

$$\frac{\Delta m}{S}_{tot} = \sqrt{k_{p\ diss} * t} + \sqrt{k_{p\ oxide} * t} = \left(\sqrt{k_{p\ diss}} + \sqrt{k_{p\ oxide}}\right) * \sqrt{t} \tag{9}$$

This leads to:

$$\frac{\Delta m}{S}_{tot} = \sqrt{k_{p\ tot} * t}\ ,\ \text{with}\ k_{p\ tot} = \left(\sqrt{k_{p\ diss}} + \sqrt{k_{p\ oxide}}\right)^2 \tag{10}$$

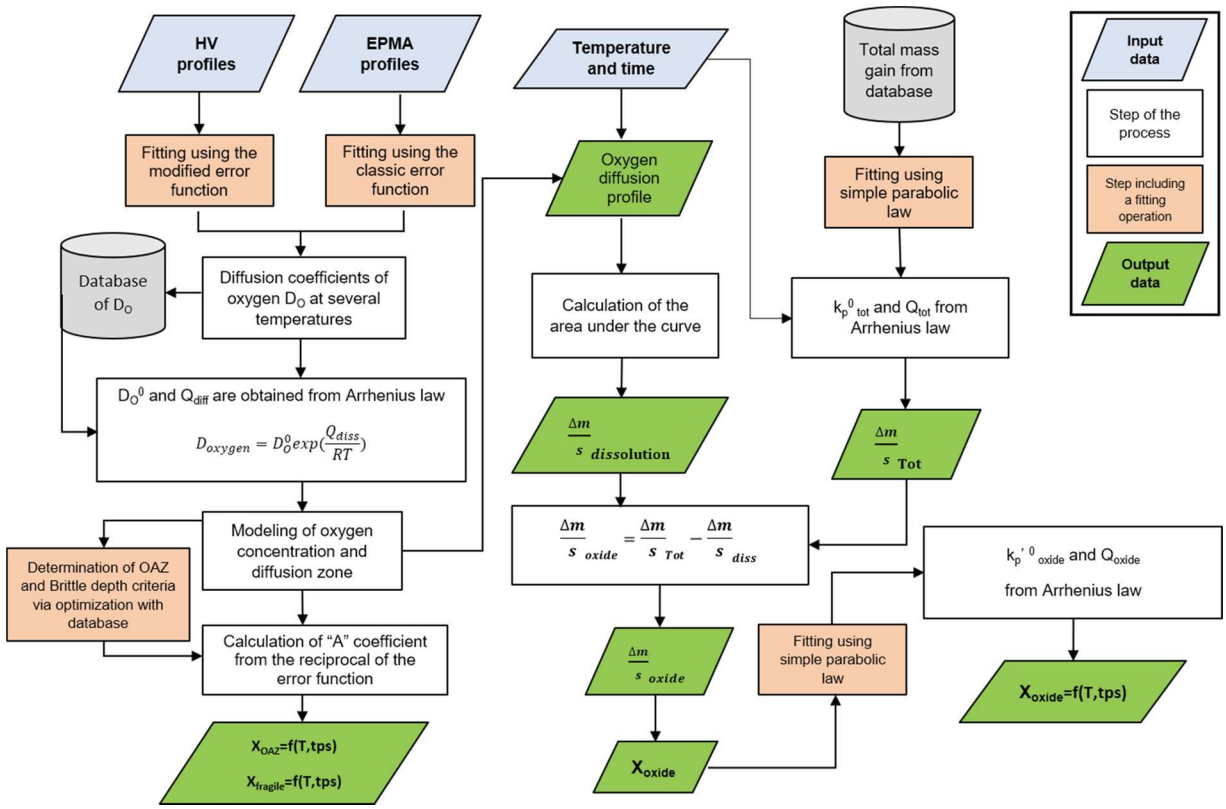


**Fig. 2.** Flowchart of the modeling.

$$Q_{tot} = -RT * ln\left[\frac{\left(\sqrt{k^0_{p\,diss} * \exp\left(\frac{-Q_{diss}}{RT}\right)} + \sqrt{k^0_{p\,oxide} * \exp\left(\frac{-Q_{oxide}}{RT}\right)}\right)^2}{k^0_{p\,tot}}\right] \quad (11)$$

Eq. (10) shows that $k_{p\,tot}$ should not follow an Arrhenius law due to the square of the sum of $\sqrt{k_{p\,diss}}$ and $\sqrt{k_{p\,oxide}}$. However, the numerical application using the coefficients determined in this study (Table 2) reveal that the difference from a linear relationship is small within the validity domain [500 °C–700 °C].

*Remark:* For the sake of clarity, in the rest of this paper, the notation $k_p$ will refer to the parabolic constant relative to mass gains expressed in $mg^2.cm^{-4}.s^{-1}$ (total, oxide and dissolution in the matrix) and $k'_p$ to the parabolic constant relative to thicknesses in $\mu m^2 s^{-1}$ (oxide scale and OAZ).

The amount of data concerning the thickness of oxide scales formed at the surface of titanium alloys as a function of time and temperature is very small. This is due firstly to the kinetics of formation of these scales, which is slow at temperatures below 600 °C [6,13,32,33], and secondly to the experimental devices required to measure these thin thicknesses. At the micrometer scale and below, observations of such layers require a scanning electron microscope (SEM-FEG) with complex surface preparations, or even a SEM equipped with a focused ion beam column (FIB-SEM) or a transmission electron microscopy (TEM) for the thinnest ones.

For each alloy, it was therefore chosen to compile experimental overall mass gains, as a function of exposure time and temperature, from the literature. A simple parabolic law (Eq. (12)) is used to model mass gain resulting from oxidation (H3):

$$\frac{\Delta m}{S}_{tot} = \sqrt{k_{p\,tot} * t} = \sqrt{k^0_{p\,tot}} * \sqrt{\exp\left(\frac{-Q_{tot}}{RT}\right) * t} \quad (12)$$

Or,

$$\frac{\Delta m}{S}_{tot} = \sqrt{k^0_{p\,tot}} * \sqrt{\theta_{tot}} \quad (12\ \prime)$$

With $\theta$, the "temperature-compensated time parameter", a Larson-Miller-like parameter, introduced by Guleryuz & Cimenoglu in their work about oxidation of Ti-64 alloy [12]. The parameter $\theta$ is used to combine both time and temperature variables into one. This parameter is useful to express the time-temperature equivalence relationship regarding the oxidation of titanium alloys and more precisely the diffusion of oxygen in the matrix of Ti-6242s and Ti-64 alloys.

A linear regression between experimental mass gain and $\sqrt{\theta_{tot}}$ is then calculated and an algorithm minimizing sums of squares (solver tool of Microsoft Excel spreadsheet) is used to find a total mass gain activation energy $Q_{tot}$ giving a coefficient of determination $R^2$ close to 1. The square root of the pre-exponential coefficient $\sqrt{k^0_{p\,tot}}$ is, in this case, directly equal to the slope of the linear regression (Eq. 12′).

The oxide scale thickness, $e_{oxide}$, is finally obtained from the mass gain due to oxide growth, assuming a dense, homogeneous and adherent oxide scale (H9):

$$Oxide\ scale\ thickness\ (\mu m) = 10 * \frac{\left(\frac{\Delta m}{S}_{tot} - \frac{\Delta m}{S}_{diss}\right) * M_{TiO2}}{\rho_{TiO2} * 2 * M_{oxygen}} \quad (13)$$

With the mass gain due to oxygen uptake in the oxide scale in $mg.cm^{-2}$, $M_{TiO2}$ and $M_{oxygen}$ in $g.mol^{-1}$ and $\rho_{TiO2}$ in $g\,cm^{-3}$.

Similarly to what was done with total mass gain data, the above calculated oxide thicknesses for various temperatures and exposure times are modeled by a simple parabolic law (14). The activation energy that properly models the calculated oxide thicknesses $Q_{oxide}$ and then

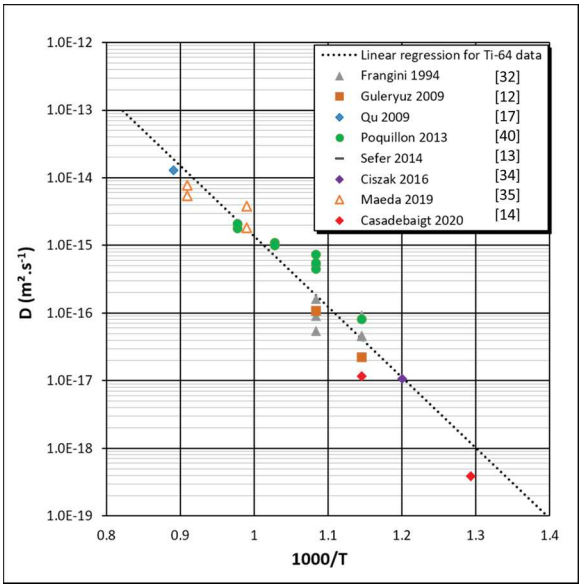


**Fig. 3.** Arrhenius diagram of apparent oxygen diffusion coefficients for t Ti-64 alloy.

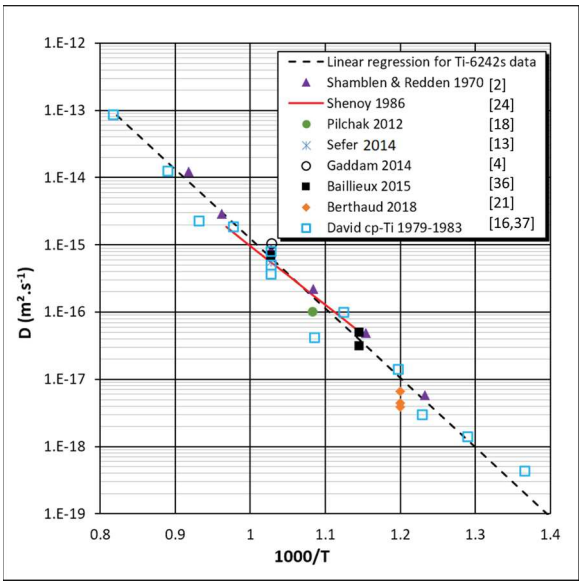


**Fig. 4.** Arrhenius diagram of apparent oxygen diffusion coefficients for Ti-6242s alloy and comparison with diffusion coefficients of oxygen in commercially-pure titanium from David et al. studies [16,37], (open blue squares). (For interpretation of the references to colour in this figure legend, the reader is referred to the web version of this article.)

$k_p{}'^{,0}_{oxide}$ are then determined by minimizing the sum of squares. Of course, this last equation accumulates all the uncertainties related to the adjustment of the apparent diffusion coefficients, OAZ depths and experimental mass gains but succeeds in obtaining a complete model composed of three independent central equations, namely Eqs. (5), (12) and (14):

$$e_{oxide} = \sqrt{k_p{}'_{oxide} * t} = \sqrt{k_p{}'^{,0}_{oxide}} * \sqrt{\exp\left(\frac{-Q_{oxide}}{RT}\right) * t} \quad (14)$$

A flowchart is proposed in Fig. 2 to summarize and better visualize the different steps of this modeling.

**Table 1**
Thermokinetics coefficients for apparent diffusion of oxygen in Ti-64, Ti-6242s and for diffusion of oxygen in commercially-pure titanium (cp-Ti) for T in [350 °C–900 °C].

| Alloy | $Q_{diss}$ (J. mol$^{-1}$) | $D_o^0$ (μm$^2$.s$^{-1}$) | Reference |
|---|---|---|---|
| Ti-64 | 199,850 | $3.83 \times 10^7$ | This work |
| Ti-6242s | 197,600 | $2.59 \times 10^7$ | This work |
| Cp-Ti | 191,100 | $8.96 \times 10^6$ | [16,37] |
| Global | 195,100 | $1.86 \times 10^7$ | This work |

**Table 2**
Modeled thermokinetics coefficients for Ti-64 and Ti-6242s.

| Coefficients | Alloy | | Reference |
|---|---|---|---|
| | Ti-64 | Ti-6242s | |
| **Co (at. %)** | 0.60 | 0.25 | [5,40] |
| **Cs (at. %)** | 25 | 25 | [36,38] |
| **$C_{OAZ}$ (at. %)** | 1.75 | 0.90 | This study |
| **$C_{Brittle}$ (at. %)** | 1 | 0.50 | [24,31] |
| **$Q_{diss}$ (J mol$^{-1}$)** | 199,850 | 197,600 | This study |
| **$D_o^0$ (μm$^2$ s$^{-1}$)** | $3.83 \times 10^7$ | $2.59 \times 10^7$ | This study |
| **$k'^0_{p\ diss}$ (μm$^2$ s$^{-1}$)** | $3.02 \times 10^8$ | $2.55 \times 10^8$ | This study |
| **$k_{p\ diss}^0$ (mg$^2$ cm$^{-4}$ s$^{-1}$)** | $7.28 \times 10^4$ | $4.12 \times 10^4$ | This study |
| **$Q_{tot}$ (J mol$^{-1}$)** | 231,600 | 244,600 | This study |
| **$k_{ptot}^0$ (mg$^2$ cm$^{-4}$ s$^{-1}$)** | $4.90 \times 10^7$ | $7.60 \times 10^7$ | This study |
| **$Q_{oxide}$ (J mol$^{-1}$)** | 273,450 | 349,050 | This study |
| **$k'^0_{p\ oxide}$ (μm$^2$ s$^{-1}$)** | $2.69 \times 10^{11}$ | $7.10 \times 10^{14}$ | This study |
| **$k_{p\ oxide}^0$ (mg$^2$ cm$^{-4}$ s$^{-1}$)** | $7.72 \times 10^9$ | $2.04 \times 10^{13}$ | This study |
| **$Q_{tot}$ (J mol$^{-1}$) calculated from** Eq. (11) | 231,500 | 243,400 | This study |

## 3. Application to Ti-64 and Ti-6242s alloys

The method proposed in the previous section was applied to Ti-64 and Ti-6242s alloys.

### 3.1. Oxygen diffusion in the alloys

Apparent oxygen diffusion coefficients, obtained from literature and analysis of EPMA and microhardness profiles, are represented in Arrhenius diagrams in Figs. 3 (Ti-64) and 4 (Ti-6242s). Most coefficients of Ti-64 alloy were obtained by reanalyzing (using Eq. (2)) the microhardness profiles available in the literature [12,13,17,32,34,35]. For Ti-6242s alloy, the diffusion coefficients mainly come from the analysis of concentration profiles (EPMA, NRA, SIMS) and are therefore directly available in the respective studies [2,24,36]. The diffusion coefficients of oxygen in commercially pure titanium (cp-Ti) determined by David et al. [16,37], have also been plotted in Fig. 4 for comparison with Ti-6242s. All the coefficients shown in these two figures are made available in Table B1 of Appendix B.

For each dataset, a linear regression was performed which gave access to the activation energy $Q_{diff}$ (J/mol) and the pre-exponential factor $D_o^0$ (μm$^2$/s) of the apparent oxygen diffusion. Despite the fact that cp-Ti data are shown together with Ti-6242s data in Fig. 4, these data were not used in the linear regression treatment and do not impact the thermokinetics coefficients subsequently determined. In addition, coefficients specific to cp-Ti were also recalculated.

All the coefficients are summarized in Table 1. It can be noticed that the values for Ti-64 and Ti-6242s alloys are very close to each other. This is also noticeable by comparing the two linear regressions showing the same evolution with temperature. This shows that the chemical composition and microstructure of these two titanium alloys have no or little influence on oxygen diffusion in the range of temperature and oxidation time in which the data were analyzed.

The plotting of cp-Ti data with Ti-6242s data (Fig. 4) confirms that the apparent diffusion of oxygen in Ti-6242s is very similar to the diffusion in the pure titanium matrix. Furthermore, these two statements

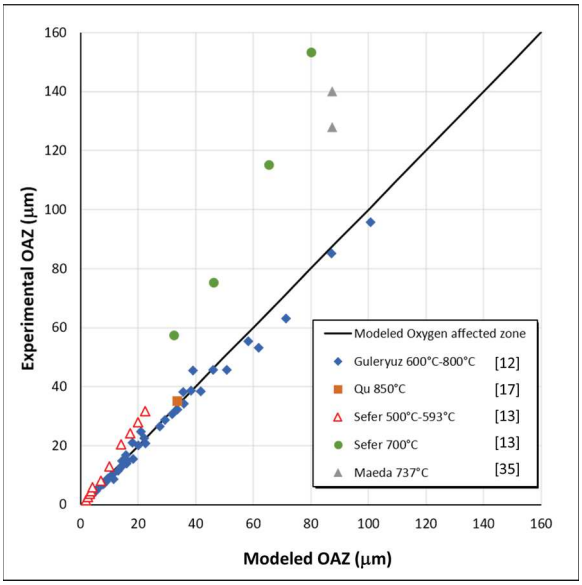


**Fig. 5.** Comparison between experimental and modeled Oxygen Affected Zone (OAZ) depths for Ti-64 alloy.

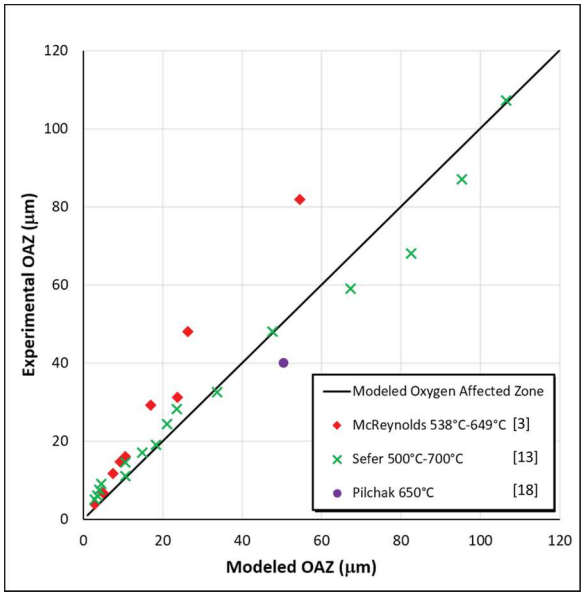


**Fig. 6.** Comparison between experimental and modeled Oxygen Affected Zone (OAZ) depths for Ti-6242s alloy.

are consistent with the results of previous studies in which it was shown that the apparent diffusion of oxygen in Ti-64 and pure titanium are comparable [22,32]. It would have been convenient to plot all the diffusion coefficients of Ti-64, Ti-6242s and cp-Ti in a single Arrhenius diagram and to extract a specific pair: activation energy, $Q_{diss,}$ and pre-exponential factor, $D_o^0$. However, for the sake of visual clarity, this plot is not proposed here but the coefficients resulting from this global linear regression are given in Table 1.

### 3.2. Modeling of the Oxygen Affected Zone (OAZ)

It can be recalled that, in this work, the oxygen affected zone or OAZ, corresponds to the "white layer" observable after chemical etching (using Kroll's reagent for example) on a polished cross section of an oxidized near-alpha titanium alloy sample. Datasets of experimental OAZ depth values were thus collected from the literature for oxidized Ti-64 [12,13,17,35], and Ti-6242s [3,13,18].

For each alloy, Eq. (6) was adjusted to experimental data using thermokinetics coefficients from Table 1 with a conventional initial oxygen contents $C_0$ equal to **0.60 at. %** for Ti-64 and **0.25 at. %** for Ti-6242. For each alloy, a unique initial oxygen concentration was chosen to simplify data treatment and because this information is rarely given accurately in the literature. Surface oxygen concentration *Cs,* which should correspond to the average oxygen concentration at the interface, i.e. the oxygen solubility limit in the matrix (H4), was taken equal to **25 at. %** for both alloys, based on experimental data [36,38]. It appears that this particular parameter is not very critical for OAZ depth modeling as the calculations carried out with the model proposed in this study showed that a variation of ±5 at. % of the concentration at the interface (taken between 20 at. % and 30 at. %) results in a difference of about ±4 % in the value of the modeled OAZ depth.

$C_{OAZ}$ values were then determined by following the procedure described in the previous part. They are found equal to **1.75 at. %** for Ti-64 and **0.90 at. %** for Ti-6242s, which leads to a constant A of **1.40** and **1.57** respectively. These values as well as $C_0$ and $C_s$ are summarized in Table 2, and comparisons between modeled and experimental OAZ depths are displayed in Figs. 5 and 6 . Lastly, the constant A of Eq. (6) can be calculated for both alloys, giving access to the modeling equations of $x_{OAZ}$ as a function of temperature and exposure duration: Eqs. (15) and (16).

*For Ti64,*

$$x_{OAZ-Ti64} = 2.80\sqrt{3.83 * 10^7 * \exp\left(\frac{-199850}{RT}\right) * t} \quad (15)$$

*For Ti6242s,*

$$x_{OAZ-Ti6242} = 3.14\sqrt{2.59 * 10^7 * \exp\left(\frac{-197600}{RT}\right) * t} \quad (16)$$

With $t$ in s and $T$ in K, Valid for $x_{OAZ}$ in [0−100µm], or T in [500−700 °C] and t in [0–300 000 h]

The comparisons between the models and the experimental data (Figs. 5 and 6) show that, for each alloy, some data could not be adjusted. This concerns the results of Sefer at 700 °C for Ti-64 [13] and McReynolds et al. for Ti-6242s [3]. In the first case, it appears that the measured diffusion zone depths are much greater than those generated by the model. No significant differences in composition, microstructural parameters or surface preparation protocol can easily explain this discrepancy. However, it can be recalled that at 700 °C, the global oxidation kinetics is expected to change from parabolic to linear, which is not the case in Sefer's study. In the case of Ti-6242s, the visible deviations between the results of McReynolds et al. and the model appear at the highest oxidation temperatures, e.g. at 649 °C (1200 °F) the measured OAZ depth is 82 µm against a modeled value of 54 µm after 500 h of oxidation. Deviations are also noticeable for the lowest temperatures with 15 µm measured against 9 µm modeled after 500 h of oxidation at 538 °C (1000 °F).

Explaining this deviation is not straightforward due to the lack of dedicated and extensive studies, but from the database built in this work, some hypotheses can be drawn. A possible explanation could be the beta phase volume fraction in the alloy used by McReynolds which was quantified at 26 %, whereas lower fractions are generally found in the literature like 14 % for Berthaud [21] or 20 % for Sefer [13]. From another perspective, it is also important to note that the composition of the alloy used by McReynolds is also slightly different from that of other Ti-6242s alloys studied in the literature. Indeed, according to the measurements available in his study, the alloy contains only 1.76 wt. % Sn, compared to higher contents of 2.3 wt. % for Berthaud and 2 wt. % for Sefer. A theoretical study based on Density Functional Theory calculations showed that addition of Sn reduces the diffusivity of oxygen as

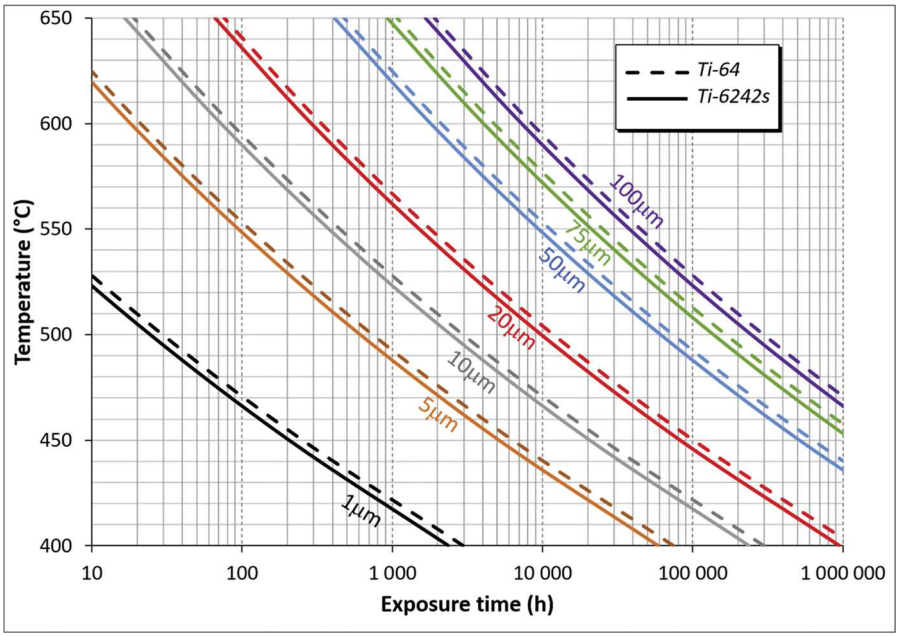


**Fig. 7.** Prediction map of several Oxygen Affected Zone (OAZ) depths as a function of temperature and exposure time for Ti-64 (dashed line) and Ti-6242s (solid line) alloys based on Eqs. (15) and (16).

compared to pure titanium but so far, no dedicated experimental study has been carried out. However, it can be noted that AMS6953, a new high temperature titanium alloy designed for an increased oxidation resistance compared to Ti-6242s at 650 °C, contains 4 wt. % Sn, i.e. twice as much as Ti-6242s [39].

With the method proposed in the present work, it is important to emphasize that the validity range of the model is limited by the most restrictive range among that of the temperatures of the diffusion coefficients used (350 °C–900 °C) and that of the datasets of experimental OAZ (500 °C–700 °C). The model has an upper limit corresponding to the highest OAZ value measured experimentally under given conditions (time and temperature). Staying within the validity range of the model means interpolating with Eq. (6) between $x_{OAZ} = 0$ µm and this maximum $x_{OAZ}$ value (100 µm). The model admits extrapolations but they should always be carried out carefully. Eq. (17), which is a rewriting of Eq. (15), makes it possible to calculate the time to reach the target OAZ depth value. For example, the model predicts that reaching a diffusion depth of 100 µm in Ti-64 alloy at 500 °C requires a duration of 300.000 h i.e. 34 years. Since the kinetics of OAZ growth increases less and less rapidly with time (parabolic law) and decreases drastically with temperature ($k_p$ following an Arrhenius law), Eqs. (17) and (18) could be used at temperatures lower than 500 °C for extended periods of time.

$$t_{x_{OAZ}-Ti64} = \left[\frac{x_{OAZ}}{2.80}\right]^2 * \left[\frac{1}{3.83*10^7 * \exp\left(\frac{-199850}{RT}\right)}\right] \quad (17)$$

Similarly, Eq. (18) is used to calculate the time required to reach an oxygen affected zone depth for Ti-6242s alloy based on Eq. (16) with $t$ in s and $T$ in K.

$$t_{x_{OAZ}-Ti6242s} = \left[\frac{x_{OAZ}}{3.14}\right]^2 * \left[\frac{1}{2.59 * 10^7 * \exp\left(\frac{-197600}{RT}\right)}\right] \quad (18)$$

These two new equations were used to build an iso-depth abacus of OAZ as a function of temperature and exposure time for the two alloys (Fig. 7) where it can be seen that the evolution of OAZ depth in Ti-64 and Ti-6242s alloys are very similar between 400 °C and 650 °C. This is consistent with the experimental observations made by Sefer on these two alloys [13]. This diagram highlights that an increase of 50 °C, from 450 °C to 500 °C, will result in an increased OAZ depth by a factor of 3.4. This factor decreases with increasing temperature and is equal to 2 for a 50 °C increase between 600 °C and 650 °C.

As previously mentioned in this paper, the available experimental data are insufficient to verify or refine the ductile-to-brittle oxygen concentration $C_{Brittle}$ and therefore the constant B in Eq. (7). Nevertheless, by using literature values (1 at. % for Ti-64 [31] and 0.5 at. % for Ti-6242s [24]) it is possible to propose modeling equations for $x_{Brittle}$ as a function of temperature and exposure duration: Eqs. (19) and (20) with $t$, in s and $T$ in K. These equations can then be tested, discussed and adjusted according to future results. From these equations it can be predicted that the thickness of the brittle layer will be roughly similar.

*For Ti64,*

$$x_{Brittle-Ti64} = 3.4\sqrt{3.83 * 10^7 * \exp\left(\frac{-199850}{RT}\right) * t} \quad (19)$$

*For Ti6242s,*

$$x_{Brittle-Ti6242} = 3.6\sqrt{2.59 * 10^7 * \exp\left(\frac{-197600}{RT}\right) * t} \quad (20)$$

The domain of validity of these equations in terms of temperatures and times are not yet known but it can be supposed that it is similar to those of Eqs. (15) and (16), i.e. T in [500–700 °C] and t in [0–300 000 h].

### 3.3. Modeling of the total mass gain kinetics

Mass gain versus time data were collected from the literature for Ti-64 [12,32,34,40], and Ti-6242s alloys [3,5,13,21,33]. For each alloy, a set of experimental mass gains was plotted as a function of the square root of $\theta$, according to Eq. (12). The total mass gain activation energy $Q_{tot}$ and the pre-exponential coefficient $k_{ptot}$ were then determined by minimizing the sum of squares and are summarized in Table 2. The comparison between each alloy's modeled and experimental total mass gain is presented in Figs. 8 and 9 , and modeling Eqs. (21) and (22) (with $t$ in s and $T$ in K) are given:

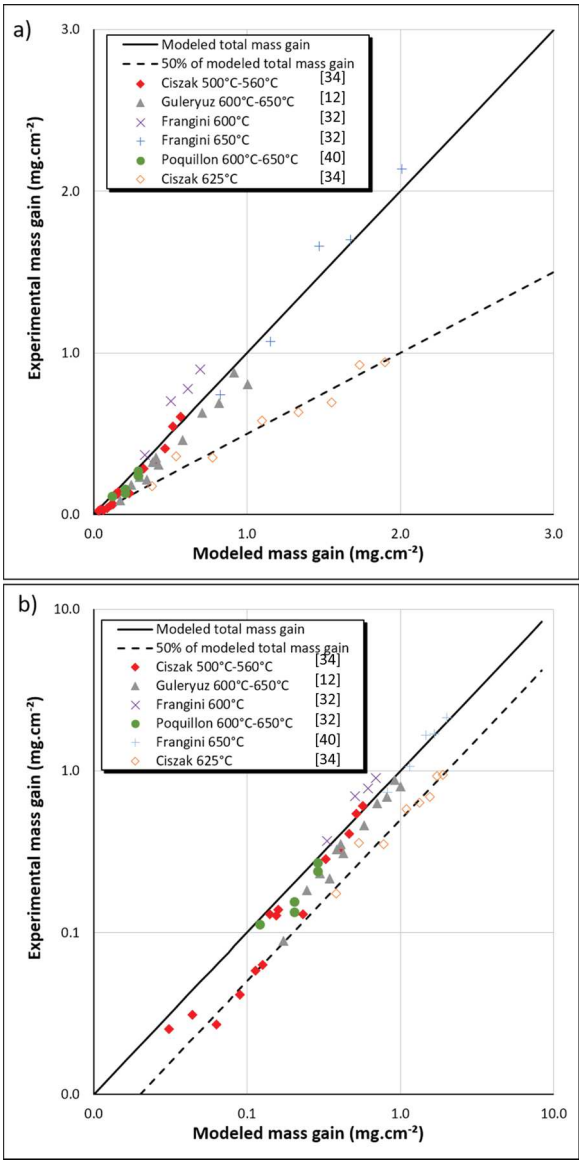


**Fig. 8.** Comparison between experimental and modeled total mass gains for Ti-64 alloy: a) using a linear scale, b) using a log-log scale.

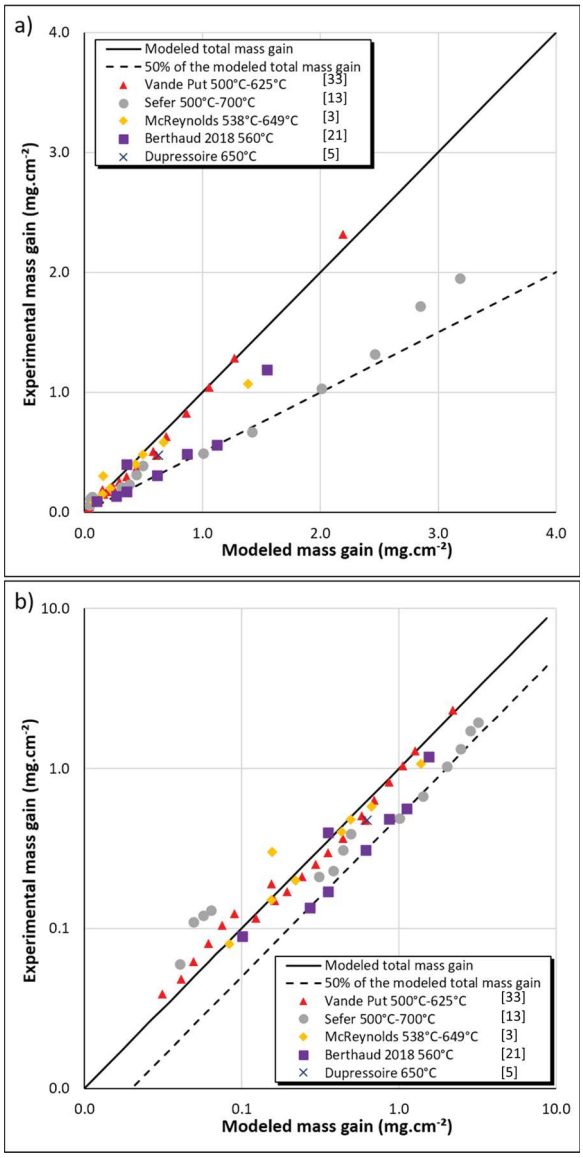


**Fig. 9.** Comparison between experimental and modeled total mass gains for Ti-6242s alloy: a) using a linear scale, b) using a log-log scale.

*For Ti64,*

$$\frac{\Delta m}{S}_{tot-Ti64} = \sqrt{4.90 * 10^7 * \exp\left(\frac{-231600}{RT}\right) * t} \quad (21)$$

*For Ti6242s,*

$$\frac{\Delta m}{S}_{tot-Ti6242} = \sqrt{7.60 * 10^7 * \exp\left(\frac{-244600}{RT}\right) * t} \quad (22)$$

Valid for $\frac{\Delta m}{S}$ in [0−2 mg.cm$^{-2}$], or T in [500−700 °C] and t in [0–300 000 h]

It should be mentioned here that, for Ti-64, not all of the experimental mass gains available in the literature were collected and some of the collected data were not used to adjust Eq. (12). Firstly, the kinetics modeled in this study all follow parabolic kinetics, which is not the case of Ti-64 alloy for temperatures above 700 °C at which the kinetics becomes linear [13]. It was therefore chosen to neither collect nor use mass gain data for temperatures above 700 °C, as in the studies of Frangini et al. [32], Sefer et al. [13] or Guleryuz et al. [12]. Secondly, it was noticed that for some data sets, it was not possible to adjust Eq. (12) so as to obtain a value of $Q_{diff}$ that could model the rest of the data correctly. This is the case of the results obtained by Ciszak et al. at 625 °C [34], whereas those obtained at 500 and 560 °C were included in the model into account. This deviation from the rest of the dataset is emphasized in Fig. 8a where a 50 % difference between the model and the data of Ciszak et al. at 625 °C can be seen. The log-log scale in Fig. 8b highlights the fact that the data relative to the lowest temperature in the same study, i.e. 500 °C, also deviates from the model by approximately 50 %.

A choice was also made regarding the mass gain data used for Ti-6242s. The only dataset that was used to adjust Eq. (10) was extracted from the study of Vande Put et al. [33] as it leads to thermokinetics coefficients giving higher parabolic constants, $k_{p\ tot}$. From our perspective it is indeed preferable for the model to slightly overestimate the total mass gain and thus the oxide scale thickness than to underestimate them by taking into account all available data. This choice is, of course, debatable. This decision is supported by Fig. 9a and b where it can be seen that the experimental mass gains of the other studies are twice as small as those predicted by the model. This choice is also justified by the fact that the data cover an extensive range of mass gains, from 0.04 mg.cm$^{-2}$ to 2.32 mg.cm$^{-2}$ for temperatures and exposure times ranging

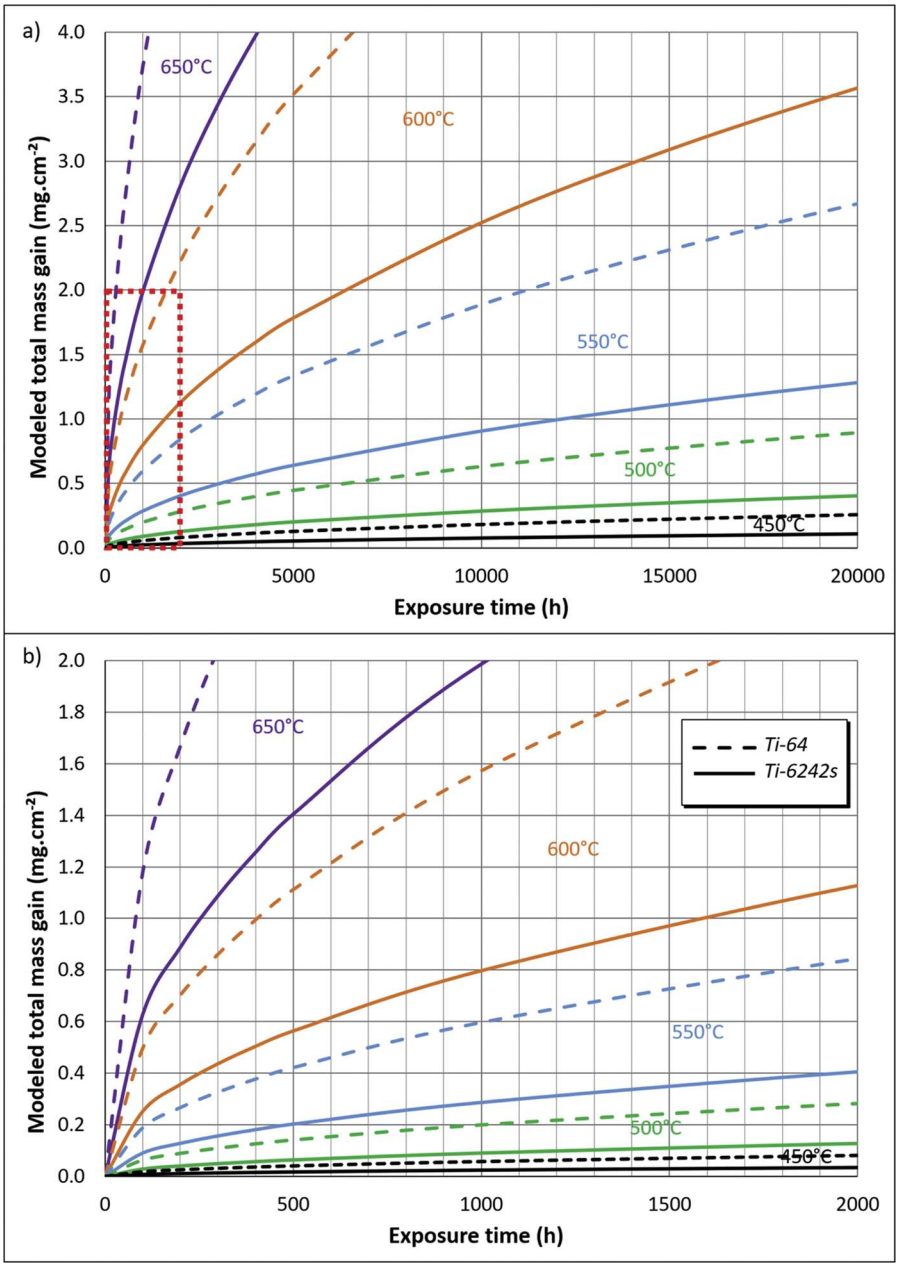


**Fig. 10.** Modeled total mass gain as a function of exposure time at various temperatures for Ti-64 (dashed line) and Ti-6242s (solid line) alloys based on Eqs. (17) and (18), a) full-scale and b) enlargement of the red dashed-line square area in a). (For interpretation of the references to colour in this figure legend, the reader is referred to the web version of this article.)

from 100 h at 500 °C to 3000 h at 625 °C.

These important discrepancies, potentially leading to a doubling of the total mass gain, hardly seem to result from small differences in alloy composition nor from surface polishing. Although the influence of polishing and, more generally, of surface roughness on oxidation kinetics has already been demonstrated for Zircaloy-4 [41], as well as for additively manufactured Ti-64 [38]. In addition, it can be noted that the data from the studies of Frangini et al. and Guleruyz et al. can be modeled by a single pair of thermokinetics coefficients despite their different surface polishing protocols (P600 and P1200 then mirror-finish respectively).

An incorrect control of the thermal homogeneity in the furnaces could also lead to the above-mentioned observation. In fact, a deviation of 25 °C is enough to explain a factor of two in the total mass gain (using the model proposed in this study). This hypothesis can be verified in practice with OAZ measurements, since a 25 °C difference leads to a 33 % difference between measured and modeled OAZ (Fig. 7). Experimental data regarding this case are, however, not available in the mentioned studies. If the total mass gains measured and predicted were very different but not the OAZ depths, the temperature parameter would probably not have an influence because the formation kinetics of OAZ seems to depend only on temperature. This statement can be supported by the small differences in OAZ depths measured by Casadebaigt et al. after oxidation of additively manufactured Ti-64 samples with and without hot isostatic pressing (HIP), i.e. with very different microstructures [38]. In this case, the mass gain difference between samples would only be explained by the thickness variation of the oxide scales formed. Some hypotheses can be proposed to explain these variations. For example, it would be interesting to study the influence of gas velocity, i.e. whether or not the furnace is equipped with air circulation. This remark is supported by the differences between the mass gains found by Vande Put et al. [33] and those found by Sefer [13] and Berthaud [21]. Again, the mass gains vary by a factor of 2 (Fig. 9) and one

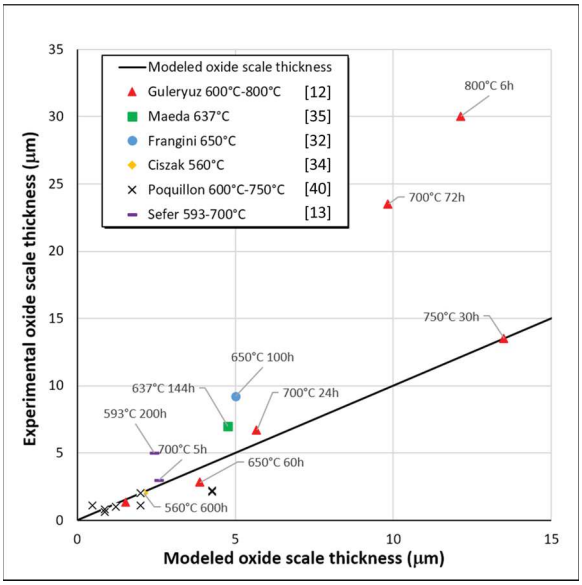


**Fig. 11.** Comparison between experimental and modeled oxide scale thicknesses Ti-64 alloy.

noticeable difference in their respective experimental protocols is the use of circulating air furnace for the former (Nabertherm N 60/85 and N 120/85) whereas Sefer used a static air furnace (Nabertherm N11/R) and Berthaud used a tubular furnace (Nabertherm RHTC 80-450/15).

Prediction curves for the evolution of the total weight gain of Ti-64 and Ti-6242s alloys as a function of time between 450 °C and 650 °C are shown in Fig. 10a, and an enlargement corresponding to an oxidation time of up to 2000 h is proposed in Fig. 10b. Oxidation duration and temperature ranges were chosen to be consistent with the validity of the model. These plots highlight that from 450 °C to 650 °C, the total mass gain ratio between Ti-64 and Ti-6242s is close to 2, and that, for both alloys, raising the temperature by 50 °C leads to an increase in total mass gain by a factor of 3.

### 3.4. Modeling of the oxide scale thickness

The total mass gains for Ti-64 and Ti-6242s were modeled for a set of temperatures (450 °C–650 °C) and exposure durations (100 h to 20.000 h) using Eqs. (19) and (20). The mass gains due to oxygen dissolution in the matrix were calculated from the areas under the oxygen concentration profiles using Eq. (4). For both alloys, the oxide scale thickness was obtained from Eq. (13). These calculated thicknesses were adjusted with a simple parabolic law thus giving access to the thermo-kinetics coefficients of Eq. (14). $Q_{oxide}$ and $k_p{}'^{0}_{oxide}$ were found equal to 273 k J mol$^{-1}$ and 2.30 × 10$^{11}$ µ m$^2$.s$^{-1}$ for Ti-64, and to 350 kJ mol$^{-1}$ and 7.10 × 10$^{11}$ µ m$^2$ s$^{-1}$ for Ti-6242s (coefficients are summarized in Table 2). The activation energy of Ti-64 is close to that of oxygen diffusion in rutile TiO2, which is between 232 and 276 kJ.mol$^{-1}$ according to the review by Liu and Welsch [42]. It can be argued that within the validity range of the model, the growth of the oxide layer at the surface of Ti-64 would indeed be limited by the diffusion of oxygen in the $TiO_2$ scale. This is consistent with the hypothesis of a dense and compact oxide made at the beginning of this study (H9), which therefore seems correct within the validity range of the model. Of course, a part of the oxygen flux that crosses the oxide scale is not consumed by the oxide scale growth, but diffuses inside the metal thereby increasing its oxygen concentration. This decreases the thickness of the oxide scale, but not enough to affect the apparent activation energy of the oxide scale growth. In contrast to Ti-64, the $Q_{oxide}$ of Ti-6242s is much higher (absolute value) than that of the diffusion of oxygen in $TiO_2$. This could confirm the beneficial effect of the minor elements, such as silicon, present in this alloy.

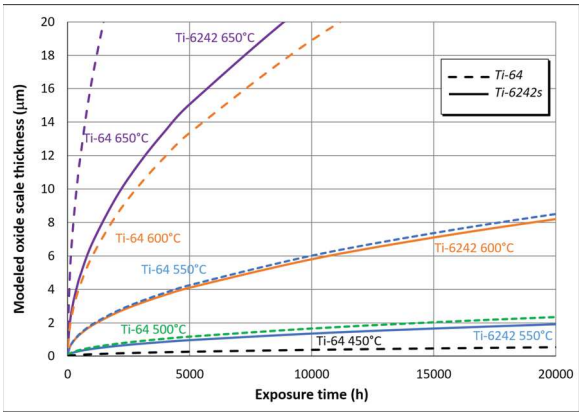


**Fig. 12.** Prediction curves of oxide scale thickness as a function of exposure time at various temperatures for Ti-64 (dashed line) and Ti-6242s (solid line) alloys based on Eqs. (19) and (20).

*For Ti64,*

$$e_{oxide-Ti64} = \sqrt{2.69 * 10^{11} * \exp\left(\frac{-273450}{RT}\right) * t} \tag{23}$$

*For Ti6242s,*

$$e_{oxide-Ti6242} = \sqrt{7.10 * 10^{14} * \exp\left(\frac{-349050}{RT}\right) * t} \tag{24}$$

With t in s and T in K. The domain of validity is the same that for the total mass gain, i.e. T in [500−700 °C] and t in [0–300 000 h].

Experimental oxide scale thicknesses gathered from the literature were compared to the model, see Fig. 11. This figure reveals that, overall, Eqs. (23) and (24) correctly model experimental data, despite the accumulation of all the uncertainties associated with the modeling of total mass gain and oxygen diffusion in the matrix. At very high temperatures and for longer oxidation times, important deviations appear. The data of Guleryuz et al. [12] clearly shows this. The model adequately reproduces the oxide thickness after 24 h of oxidation at 700 °C but a significant deviation appears after 72 h of oxidation (23 µm against 10 µm). This deviation from the parabolic model is not surprising and seems to be linked to the change in oxidation kinetics regime – from parabolic to linear – that has been verified experimentally at higher temperatures (800 °C–1200 °C) by Kofstad et al. [43]. This particular point will be discussed later in the section on the limitations of the model.

The variations in oxide scale thicknesses of both alloys as a function of time and for several temperatures, calculated from Eqs. (23) and (24), are shown in Fig. 12. Compared to chromino-forming [44] and especially alumino-forming alloys [45], titanium alloys have high overall oxidation kinetics and oxide scale growth kinetics. However, as the temperatures associated with titanium use in aerospace applications are relatively moderate, the metal consumption of titanium alloys remains low, especially for Ti-6242s. For this alloy, the modeled oxide scale after 20.000 h of oxidation at 600 °C would be 8 µm thick and for temperatures lower than 550 °C, it would be 2 µm thick. Since the oxidation kinetics is parabolic (in the validity range of the model), it can be argued that, for extremely long periods of several hundred thousand hours such as those found in the aeronautics industry (an ultra-long haul of the Airbus A350−1000 every day for 30 years corresponds to 220.000 h), the formation of the oxide layer on a part exposed to temperatures below 550 °C does not appear to be life-limiting. Secondly, Fig. 12 shows that the difference between the two alloys modeled is greater for oxide scale thicknesses than for mass gains at low temperatures and tends to decrease with higher temperatures. This is due to the fact that the

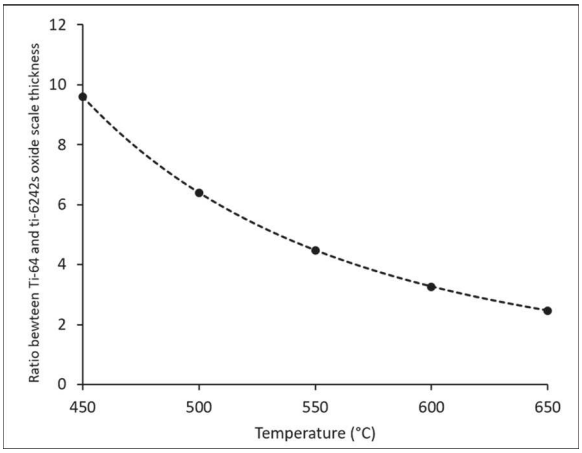


**Fig. 13.** Ratio between Ti-64 and Ti-6242s oxide scale thickness as a function of temperature.

activation energy of oxide scale formation $Q_{oxide}$ ofTi-6242s is higher than that of Ti-64. The evolution of the ratio between Ti-64 and Ti-6242s oxide layers formed is presented in Fig. 13; its value varies from 10 at 450 °C to 2.5 at 650 °C. Finally, it can be seen in Fig. 12 that the difference between Ti-64 and Ti-6242s oxide layer growth kinetics corresponds to a 50 °C shift. For example, the kinetics of Ti-64 at 550 °C is equivalent to that of Ti-6242s at 600 °C.

Predicted oxide thicknesses can also be superimposed on oxygen affected zone depths. This abacus was plotted for Ti-64 in Fig. 14 where OAZ thicknesses are in dashed lines and oxide layer thicknesses in solid lines. This type of mapping can be used to design oxidation experiments, to predict the lifetime of a part or to optimize the parameters of surface heat treatments. From the analysis of Fig. 14 and based on the criteria of oxygen affected zone depth and oxide layer thickness, it can be suggested that the use of Ti-64 for long term applications at temperatures below 500 °C would be possible. Indeed, the diffusion in the Ti-64 matrix is very close to that found in Ti-6242s and, as an example, the modeled thickness of the oxide layer for Ti-64 would only slightly exceed 10 µm after 200.000 h at 500 °C. This seems nonrestrictive compared to the 100 µm depth of the OAZ. Needless to say that, at these temperatures, these criteria are secondary behind mechanical strength, fatigue and creep.

### 3.5. *Arrhenius diagrams*

The thermokinetics coefficients determined throughout the application section lead to two Arrhenius diagrams related to the oxidation kinetics of Ti-64 and Ti-6242s (Figs. 15 and 16 ). On each diagram the evolution of the three parabolic constants $k_{p\ tot}$, $k_{p\ oxide}$ and $k_{p\ diss}$ (total mass gain, oxide layer and oxygen dissolution in the matrix), calculated using pre-exponential factors $k_p^0$ and activating energies $Q$ from Table 2, are plotted on a logarithmic scale (left axis). The contribution of each phenomenon, given as a percentage of the total mass gain, is represented by cumulative areas (linear scale on the right axis gives the proportion due to dissolution). All others thermokinetics coefficients determined through this study as well as the mean values of the activation energies of the total mass gain ($Q_{tot}$) calculated from Eq. (11) are also given in Table 2. These are in excellent agreement with the experimentally determined values, which shows the consistency among the different data modeled in this study.

## 4. Limitations of the model

As this model consists of parabolic equations that can easily be inserted in any spreadsheet, it should be reminded that it has limitations and that these could be used as a basis for future studies.

The main limitation of the model can be found at high temperatures, i.e. above 600 °C, and very long exposure times; this challenges hypotheses H5 (negligible oxide/metal interface displacement) and H9 (dense oxide). Under these conditions, the growth of the oxide may become non-negligible compared to the OAZ thickness and it would no longer be possible to neglect the displacement of the metal/oxide interface. Since the oxide scale grows to the detriment of the metal, it affects OAZ growth kinetics, as shown numerically by Ciszak et al. [28]. Because hypothesis H5 is no longer valid, the modeled OAZ depths and oxide thicknesses may then no longer be representative of the behavior found through experimental measurements. Moreover, the model assumes that the oxide is dense and undamaged throughout its growth

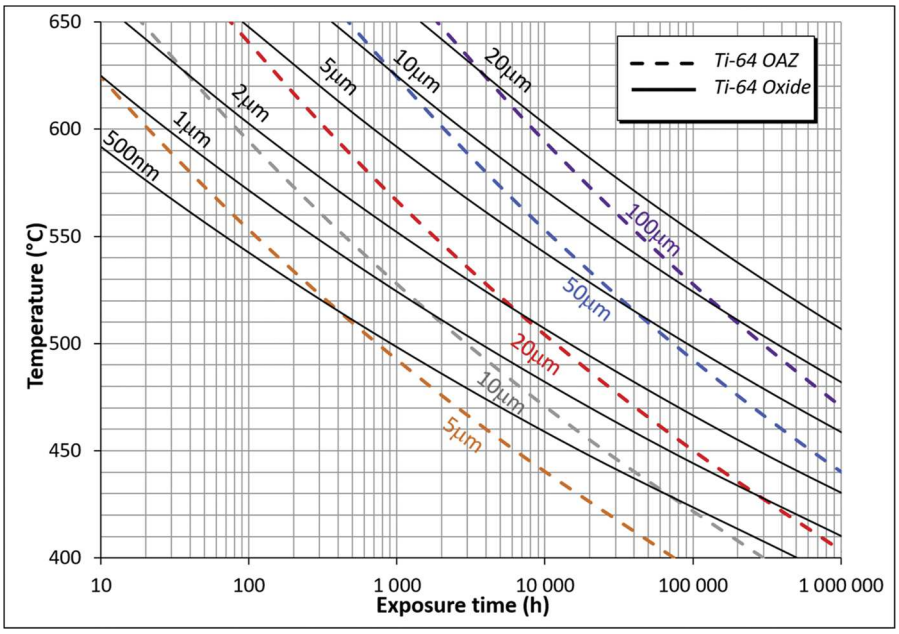


**Fig. 14.** Combined prediction map of several Oxygen Affected Zone (OAZ) depths (dashed line) and oxide scale thicknesses (solid lines) as a function of temperature and exposure time for Ti-64 based on Eqs. (15) and (19).

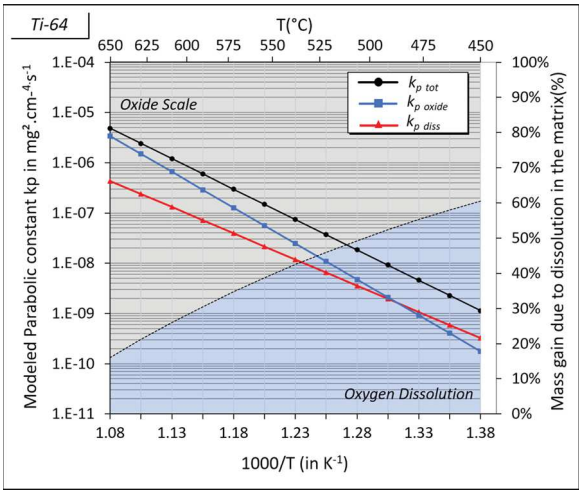


**Fig. 15.** Arrhenius diagram of the modeled mass gain for Ti-64 alloy (Y-axis in log-scale): parabolic constant for total mass gain is in black line and round marks, parabolic constant of mass gain due to oxide scale formation in blue line and square marks and parabolic constant of mass gain due to oxygen dissolution in the matrix in red line and triangle marks. The proportion of total mass gain due to dissolution is given in percentage through cumulated colored areas (grey for oxide and blue for dissolution). The proportion due to the oxide layer is equal to the difference as compared to.100 %. (For interpretation of the references to colour in this figure legend, the reader is referred to the web version of this article.)

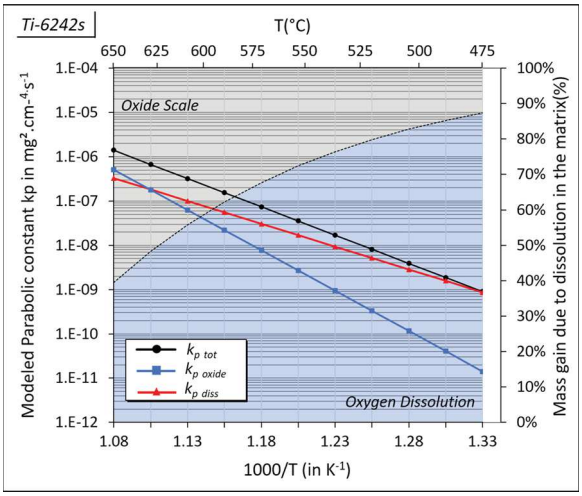


**Fig. 16.** Arrhenius diagram of the modeled mass gain for Ti-6242s alloy (Y-axis in log scale): parabolic constant for total mass gain is in black line and round marks, parabolic constant of mass gain due to oxide scale formation in blue line and square marks and parabolic constant of mass gain due to oxygen dissolution in the matrix in red line and triangle marks. The Proportion of total mass gain due to dissolution is given in percentage through cumulated colored areas (grey for oxide and blue for dissolution). The proportion due to the oxide layer is equal to the difference as compared to.100 %. (For interpretation of the references to colour in this figure legend, the reader is referred to the web version of this article.)

(H9). For sufficiently large thicknesses a cracking or even a layering of the oxide scale could appear, thereby leading to the formation of a new oxide at the metal surface. This would result in an increase in overall oxidation kinetics and even in a regime transition from parabolic to linear [46]. Such a deviation leads to an incompatibility between the predictions of the model and the experimental values. The occurrence of this phenomenon at lower temperatures for very long exposure times cannot be excluded but could not be verified due to the lack of experimental data, which would require experiments lasting hundreds of thousands of hours. Parabolic to linear kinetics transitions have been studied by Kofstad et al. through the oxidation of pure titanium between 800−1200 °C under 1 atm of $O_2$ [43] and the transition time at 900 °C was found to be of 1 h only, which is extremely short. By extrapolating their results to lower temperatures, the transition time would take place after 7000 h at 550 °C, 50.000 h at 500 °C and more than 450.000 h at 450 °C which seems compatible with the established validity range of our model and roughly reveals its limitations.

Neglecting the oxide/metal interface displacement can also lead to a mismatch between the model and experimental results in the case of oxidation of very thin samples. Indeed, when the diffusion profile reaches half the thickness of the sample, not taking into account the interface displacement would lead to an error in the diffusion coefficient in the alloy. Simple models such as the one presented in this paper are then no longer sufficient and more complete models have to be considered: complex models such as the one designed by Wagner [47] or numerical models such as the one proposed by Ciszak et al. which discusses oxidation of thin samples in detail [28].

Lastly, it is important to mention that Eqs. (15) to (24) should not be used as a linear cumulative damage rule to predict cycles involving several temperatures and exposure times even if this approach has already been presented by some authors [15]. Cumulating different exposure times and temperatures is equivalent to considering a system that returns to the starting point each time, i.e. without any history effect. To our knowledge, the open literature does not include experimental data on oxidation kinetics after complex cycles involving several temperatures which would help in checking the validity of a thermal cycling model.

## 5. Conclusions

Based on experimental data published in the literature, an empirical and analytical model has been proposed for the oxidation kinetics of Ti-64 and Ti-6242s alloys in air. This model is based on three simple parabolic laws that model the depth of the oxygen affected zone, observed experimentally as the "white layer", the total mass gain and the thickness of the oxide formed. This method, summarized in Fig. 2, should be adaptable to other near-alpha or alpha-beta titanium alloys. Beta-metastable alloys are excluded here because the phase transformations taking place during prolonged temperature exposition make the analysis of the experimental results more challenging.

The analysis of apparent diffusion coefficients shows that the diffusion of oxygen in the two alloys is similar, and not very different from the diffusion in cp-Ti. This is consistent with the fact that for equilibrium temperatures of 400 °C–600 °C, the fraction of alpha phase in the two alloys is very high, exceeding 90 vol %. It shows also that the alloying elements in solution in these two alloys do not modify the diffusion of oxygen in the alpha phase. The predictions relative to the depth of the diffusion zone in these two alloys are therefore very similar. Experimental total mass gains show that the overall oxidation kinetics of Ti-64 is faster than that of Ti-6242s. The diffusion in the alloys being similar, the main difference between these two alloys is their oxide layer growth kinetics. The fact that Ti-6242s exhibits slow kinetics of oxide layer formation leads to the conclusion that layer growth is not a limiting factor for its use in long-lasting expositions, such as those found in aerospace applications. The use of Ti-64 at temperatures above 350 °C is obviously not recommended because of its poor mechanical resistance. However, this study shows that from an oxidation resistance point of view, it could be used at temperatures as high as 550 °C. The difference in oxide layer growth between the two alloys, together with their similar OAZ depth confirm that the external oxide layer plays no role in the protection against oxygen dissolution. This result is consistent with the fact that oxygen diffusion profile is only controlled by the oxygen solubility limit at the metal/oxide interface and by the oxygen diffusion in

**Table B1**
Apparent Oxygen diffusion coefficient of Ti-6242 and Ti-64 obtained from the literature and reassessment of microhardness profiles using Eq. (2).

| Alloy | Temp. (K) | Time (h) | D ($m^2$/sec) | | Data source | Reanalyzed | Ref. |
|---|---|---|---|---|---|---|---|
| Ti-64 | 873 | 72 | 2.23 | $\times 10^{-17}$ | hardness profile | fitted with (2) | [12] |
| Ti-64 | 923 | 72 | 1.07 | $\times 10^{-16}$ | hardness profile | fitted with (2) | [12] |
| Ti-64 | 873 | 45 | 9.16 | $\times 10^{-17}$ | hardness profile | fitted with (2) | [32] |
| Ti-64 | 873 | 103 | 4.63 | $\times 10^{-17}$ | hardness profile | fitted with (2) | [32] |
| Ti-64 | 873 | 195 | 4.49 | $\times 10^{-17}$ | hardness profile | fitted with (2) | [32] |
| Ti-64 | 923 | 48.7 | 1.62 | $\times 10^{-16}$ | hardness profile | fitted with (2) | [32] |
| Ti-64 | 923 | 201 | 5.41 | $\times 10^{-17}$ | hardness profile | fitted with (2) | [32] |
| Ti-64 | 923 | 290 | 9.14 | $\times 10^{-17}$ | hardness profile | fitted with (2) | [32] |
| Ti-64 | 1010 | 144 | 1.81 | $\times 10^{-15}$ | hardness profile | fitted with (2) | [35] |
| Ti-64−1Si | 1010 | 144 | 3.82 | $\times 10^{-15}$ | hardness profile | fitted with (2) | [35] |
| Ti-64 | 1100 | 144 | 5.46 | $\times 10^{-15}$ | hardness profile | fitted with (2) | [35] |
| Ti-64−1Si | 1100 | 144 | 7.81 | $\times 10^{-15}$ | hardness profile | fitted with (2) | [35] |
| Ti-64 | 1123 | 2 | 1.29 | $\times 10^{-14}$ | hardness profile | fitted with (2) | [17] |
| Ti-64 | 873 | 3 | 8 | $\times 10^{-17}$ | SIMS profile | | [40] |
| Ti-64 | 923 | 3 | 7.3 | $\times 10^{-16}$ | SIMS profile | | [40] |
| Ti-64 | 923 | 6 | 5.2 | $\times 10^{-16}$ | SIMS profile | | [40] |
| Ti-64 | 923 | 3 | 4.5 | $\times 10^{-16}$ | SIMS profile | | [40] |
| Ti-64 | 923 | 6 | 5.5 | $\times 10^{-16}$ | SIMS profile | | [40] |
| Ti-64 | 973 | 3 | 1.1 | $\times 10^{-15}$ | SIMS profile | | [40] |
| Ti-64 | 973 | 3 | 1 | $\times 10^{-15}$ | SIMS profile | | [40] |
| Ti-64 | 1023 | 3 | 1.8 | $\times 10^{-15}$ | SIMS profile | | [40] |
| Ti-64 | 1023 | 3 | 2.1 | $\times 10^{-15}$ | SIMS profile | | [40] |
| Ti-64 | 1123 | 2 | 1.29 | $\times 10^{-14}$ | hardness profile | fitted with (2) | [17] |
| Ti-64 | 833 | 600 | 1.06 | $\times 10^{-17}$ | hardness profile | fitted with (2) | [34] |
| Ti-64 ELI | 773 | 2000 | 3.92 | $\times 10^{-19}$ | EPMA profile | | [14] |
| Ti-64 ELI | 873 | 500 | 1.17 | $\times 10^{-17}$ | EPMA profile | | [14] |
| Ti-6242s | 973 | 500 | 1.04 | $\times 10^{-15}$ | hardness profile | fitted with (2) | [4] |
| Ti-6242s | 873 | 1000 | 6 | $\times 10^{-17}$ | EPMA profile | | [36] |
| Ti-6242s | 873 | 1000 | 3.18 | $\times 10^{-17}$ | hardness profile | fitted with (2) | [36] |
| Ti-6242s | 873 | 2635 | 5 | $\times 10^{-17}$ | EPMA profile | | [36] |
| Ti-6242s | 973 | 170 | 7 | $\times 10^{-16}$ | EPMA profile | | [36] |
| Ti-6242 | 923 | 420 | 1.01 | $\times 10^{-16}$ | hardness profile | fitted with (2) | [18] |
| Ti-6242 | 973 | 500 | 5.55 | $\times 10^{-16}$ | hardness profile | fitted with (2) | [13] |
| Ti-6242 | 811 | | 5.81 | $\times 10^{-18}$ | EPMA profile | | [2] |
| Ti-6242 | 866 | | 4.98 | $\times 10^{-17}$ | EPMA profile | | [2] |
| Ti-6242 | 922 | | 2.21 | $\times 10^{-16}$ | EPMA profile | | [2] |
| Ti-6242 | 973 | | 8.57 | $\times 10^{-16}$ | EPMA profile | | [2] |
| Ti-6242 | 1039 | | 2.91 | $\times 10^{-15}$ | EPMA profile | | [2] |
| Ti-6242 | 1089 | | 1.23 | $\times 10^{-14}$ | EPMA profile | | [2] |
| Ti-6242 | 866 | | 4.3 | $\times 10^{-17}$ | EPMA profile | | [24] |
| Ti-6242 | 894 | | 8.9 | $\times 10^{-17}$ | EPMA profile | | [24] |
| Ti-6242 | 922 | | 1.8 | $\times 10^{-16}$ | EPMA profile | | [24] |
| Ti-6242 | 950 | | 3.3 | $\times 10^{-16}$ | EPMA profile | | [24] |
| Ti-6242 | 977 | | 6 | $\times 10^{-15}$ | EPMA profile | | [24] |
| Ti-6242 | 1005 | | 1.1 | $\times 10^{-15}$ | EPMA profile | | [24] |
| Ti-6242 | 1033 | | 1.8 | $\times 10^{-15}$ | EPMA profile | | [24] |
| Ti-6242s | 833 | 1000 | 1.59 | $\times 10^{-17}$ | hardness profile | fitted with (2) | [21] |
| Ti-6242s | 833 | 3000 | 6.65 | $\times 10^{-18}$ | hardness profile | fitted with (2) | [21] |
| Ti-6242s | 833 | 6000 | 4.43 | $\times 10^{-18}$ | hardness profile | fitted with (2) | [21] |
| Ti-6242s | 833 | 10,000 | 3.86 | $\times 10^{-18}$ | hardness profile | fitted with (2) | [21] |
| Ti-6242s | 898 | 3000 | 4.46 | $\times 10^{-17}$ | hardness profile | fitted with (2) | [22] |
| Cp-Ti | 1223 | 3 | 8.50 | $\times 10^{-14}$ | NRA profile | | [37] |
| Cp-Ti | 1123 | 160 | 1.25 | $\times 10^{-14}$ | NRA profile | | [37] |
| Cp-Ti | 1073 | 160 | 2.24 | $\times 10^{-15}$ | NRA profile | | [37] |
| Cp-Ti | 1023 | 72 | 1.84 | $\times 10^{-15}$ | NRA profile | | [37] |
| Cp-Ti | 973 | 502 | 5.00 | $\times 10^{-16}$ | NRA profile | | [37] |
| Cp-Ti | 973 | 160 | 3.70 | $\times 10^{-16}$ | NRA profile | | [37] |
| Cp-Ti | 973 | 2 | 8.00 | $\times 10^{-16}$ | NRA profile | | [16] |
| Cp-Ti | 921 | 4 | 4.2 | $\times 10^{-17}$ | NRA profile | | [16] |
| Cp-Ti | 889 | 20 | 1.00 | $\times 10^{-16}$ | NRA profile | | [16] |
| Cp-Ti | 835 | 88 | 1.40 | $\times 10^{-17}$ | NRA profile | | [16] |
| Cp-Ti | 813 | 71 | 3.00 | $\times 10^{-18}$ | NRA profile | | [16] |
| Cp-Ti | 775 | 50 | 1.40 | $\times 10^{-18}$ | NRA profile | | [16] |
| Cp-Ti | 732 | 72 | 4.30 | $\times 10^{-19}$ | NRA profile | | [16] |
| Cp-Ti | 673 | | 1.36 | $\times 10^{-20}$ | NRA profile | | [37] |
| Cp-Ti | 623 | | 7.73 | $\times 10^{-22}$ | NRA profile | | [37] |
| Cp-Ti | 573 | | 2.66 | $\times 10^{-23}$ | NRA profile | | [37] |

the titanium lattice.

In order to proposed more precise modeling of brittle layer depths, several options can be considered to determine the concentration values of the ductile-to-brittle transition. One of them would be to measure brittle cracks depths after room temperature tensile test, and to adjust them with Eq. (7). Another one would be to determine directly this concentration at the tip of the cracks using analytical methods such as Castaing's microprobe (EPMA) or Secondary Ion Mass Spectrometry (SIMS). This would lead to a better estimation of the difference in performance between the two alloys.

To conclude, when studying the oxidation of titanium alloys, the comparison of mass gains alone is not sufficient, although it is often used to characterize the oxidation resistance of titanium alloys in the industrial and academic fields.

## Data availability

The raw/processed data required to reproduce the work presented herein are available from the corresponding authors upon reasonable request.

## CRediT authorship contribution statement

**N. Vaché:** Conceptualization, Methodology, Validation, Formal analysis, Investigation, Writing - original draft, Writing - review & editing, Visualization. **Y. Cadoret:** Conceptualization, Funding acquisition, Writing - review & editing. **B. Dod:** Conceptualization, Funding acquisition, Writing - review & editing. **D. Monceau:** Conceptualization, Validation, Writing - review & editing, Supervision, Project administration, Funding acquisition.

## Declaration of Competing Interest

None.

## Acknowledgements

This work was financially supported by the CIRIMAT laboratory and Airbus commercial SAS.

## Appendix A

Full expression of the constants A (Eq. (A1)) and B (Eq. (A2)) required to estimate OAZ and brittle layer thicknesses as a function of oxidation temperature and duration [48]:

$$A = \left[ -\frac{2}{\pi * 0.147} - \frac{\ln\left(1-\left(1-\frac{C_{OAZ}-C_0}{C_s-C_0}\right)^2\right)}{2} + \sqrt{\left(\frac{2}{\pi * 0.147} + \frac{\ln\left(1-x\left(1-\frac{C_{OAZ}-C_0}{C_s-C_0}\right)^2\right)}{2}\right)^2 - \frac{1}{0.147}\ln\left(1-\left(1-\frac{C_{OAZ}-C_0}{C_s-C_0}\right)^2\right)} \right]^{\frac{1}{2}} \quad \text{(A.1)}$$

$$B = \left[ -\frac{2}{\pi * 0.147} - \frac{\ln\left(1-\left(1-\frac{C_{brittle}-C_0}{C_s-C_0}\right)^2\right)}{2} + \sqrt{\left(\frac{2}{\pi * 0.147} + \frac{\ln\left(1-x\left(1-\frac{C_{brittle}-C_0}{C_s-C_0}\right)^2\right)}{2}\right)^2 - \frac{1}{0.147}\ln\left(1-\left(1-\frac{C_{brittle}-C_0}{C_s-C_0}\right)^2\right)} \right]^{\frac{1}{2}} \quad \text{(A.2)}$$

## Appendix B

## Appendix C. Supplementary data

Supplementary material related to this article can be found, in the online version, at doi:https://doi.org/10.1016/j.corsci.2020.109041.

## References

[1] M. Orlita, Consommation mondiale de titane, Planétoscope. https://www.planetoscope.com/matieres-premieres/1321-consommation-mondiale-de-titane.html (consulté le mai 04, 2020).
[2] C.E. Shamblen, T.K. Redden, Air contamination and embrittlement of titanium alloys, in: R.I. Jaffe, N.E. Promisel (Eds.), The Science, Technology and Application of Titanium, 1970, pp. 199–208.
[3] K.S. McReynolds, S. Tamirisakandala, A study on alpha-case depth in Ti-6Al-2Sn-4Zr-2Mo, Metall. Mater. Trans. A 42 (7) (2011) 1732–1736, https://doi.org/10.1007/s11661-011-0710-3, juill.
[4] R. Gaddam, B. Sefer, R. Pederson, M.-L. Antti, Oxidation and alpha-case formation in Ti–6Al–2Sn–4Zr–2Mo alloy, Mater. Charact. 99 (2015) 166–174, https://doi.org/10.1016/j.matchar.2014.11.023.
[5] C. Dupressoire, A. Rouaix-Vande Put, P. Emile, C. Archambeau-Mirguet, R. Peraldi, D. Monceau, Effect of nitrogen on the kinetics of oxide scale growth and of oxygen dissolution in the Ti6242S titanium-based alloy, Oxid. Met. 87 (3–4) (2017) 343–353, https://doi.org/10.1007/s11085-017-9729-1.
[6] M. Berthaud, I. Popa, R. Chassagnon, O. Heintz, J. Lavková, S. Chevalier, Study of titanium alloy Ti6242S oxidation behaviour in air at 560 °C: Effect of oxygen dissolution on lattice parameters, Corros. Sci. 164 (2020) 108049, https://doi.org/10.1016/j.corsci.2019.06.004, mars.
[7] W.L. Finlay, J.A. Snyder, Effects of three interstitial solutes (nitrogen, oxygen, and carbon) on the mechanical properties of high-purity, alpha titanium, JOM 2 (2) (1950) 277–286, https://doi.org/10.1007/BF03399001.
[8] S. Malinov, P. Markovsky, W. Sha, Z. Guo, Resistivity study and computer modelling of the isothermal transformation kinetics of Ti–6Al–4V and Ti–6Al–2Sn–4Zr–2Mo–0.08Si alloys, J. Alloys. Compd. 314 (1–2) (2001) 181–192, https://doi.org/10.1016/S0925-8388(00)01227-5, janv.
[9] L. Bendersky, A. Rosen, The effect of exposure on the mechanical properties of the Ti-6Al-4V alloy, Eng. Fract. Mech. 20 (2) (1984) 303–311.
[10] D.P. Satko, et al., Effect of microstructure on oxygen rich layer evolution and its impact on fatigue life during high-temperature application of α/β titanium, Acta Mater. 107 (2016) 377–389, https://doi.org/10.1016/j.actamat.2016.01.058.
[11] M.S. Kalienko, M.O. Leder, A.V. Volkov, A.V. Zhelnina, P.E. Panfilov, Deformation behavior of a VT18U titanium alloy in the oxidized state, Russ. Metall. Met. 2020 (4) (2020) 325–329, https://doi.org/10.1134/S0036029520040114, avr.
[12] H. Guleryuz, H. Cimenoglu, Oxidation of Ti–6Al–4V alloy, J. Alloys. Compd. 472 (1–2) (2009) 241–246, https://doi.org/10.1016/j.jallcom.2008.04.024.
[13] B. Sefer, Oxidation and Alpha-case Phenomena in Titanium Alloys Used in Aerospace Industry: Ti-6Al-2Sn-4Zr-2Mo and Ti-6Al-4V, Luleå University of Technology, Luleå, 2014.
[14] A. Casadebaigt, J. Hugues, D. Monceau, High temperature oxidation and embrittlement at 500–600 °C of Ti-6Al-4V alloy fabricated by laser and electron beam melting, Corros. Sci. (2020) 108875, https://doi.org/10.1016/j.corsci.2020.108875, juill.
[15] I. Gurappa, Prediction of titanium alloy component life by developing an oxidation model, J. Mater. Sci. Lett. 2 (2003) 771–774.

[16] D. David, G. Beranger, E.A. Garcia, A study of the diffusion of oxygen in alpha-titanium oxidized in the temperature range 460°C-700°C, J. Electrochem. Soc. 130 (6) (1983) 4.
[17] J. Qu, P.J. Blau, J.Y. Howe, H.M. Meyer III, Oxygen diffusion enables anti-wear boundary film formation on titanium surfaces in zinc-dialkyl-dithiophosphate (ZDDP)-containing lubricants, Scr. Mater. 60 (10) (2009) 886–889, https://doi.org/10.1016/j.scriptamat.2009.02.009.
[18] A.L. Pilchak, W.J. Porter, R. John, Room temperature fracture processes of a near-α titanium alloy following elevated temperature exposure, J. Mater. Sci. 47 (20) (2012) 7235–7253, https://doi.org/10.1007/s10853-012-6673-y.
[19] B. Sefer, J. J. Roa, A. Mateo, R. Pederson, M.-L. Antti, Evaluation of the Bulk and Alpha-Case Layer Properties in Ti-6Al-4V at Micro-And Nano-Metric Length Scale, Proceedings of the 13th World Conference on Titanium, V. Venkatesh, A. L. Pilchak, J. E. Allison, S. Ankem, R. Boyer, J. Christodoulou, H. L. Fraser, M. A. Imam, Y. Kosaka, H. J. Rack, A. Chatterjee, A. Woodfield, Éd. Hoboken, USA: John Wiley & Sons, Inc., 2016, p. 1619-1624.
[20] E. Dong, W. Yu, Q. Cai, Alpha-case kinetics and high temperature plasticity of Ti-6Al-4V alloy oxidized in different phase regions, Procedia Eng. 207 (2017) 2149–2154, https://doi.org/10.1016/j.proeng.2017.10.973.
[21] M. Berthaud, Étude du Comportement de l'alliage de Titane Ti6242S à Haute Température Sous Atmosphères Complexes: Applications Aéronautiques, Université de Bourgogne Franche-Compté, Dijon, 2018.
[22] N. Vaché, D. Monceau, Oxygen diffusion modeling in titanium alloys: new elements on the analysis of microhardness profiles, Oxid. Met. (2020), https://doi.org/10.1007/s11085-020-09956-9 janv.
[23] P. Kofstad, K. Hauffe, Oxydation von titan, Mater. Corros. Korros. 7 (11) (1956) 642–649, https://doi.org/10.1002/maco.19560071107, nov.
[24] R.N. Shenoy, J. Unnam, R.K. Clark, Oxidation and embrittlement of Ti-6Al-2Sn-4Zr-2Mo alloy, Oxid. Met. 26 (1–2) (1986) 105–124, https://doi.org/10.1007/BF00664276.
[25] J. Unnam, R.N. Shenoy, R.K. Clark, Oxidation of commercial purity titanium, Oxid. Met. 26 (3–4) (1986) 231–252, https://doi.org/10.1007/BF00659186.
[26] T. Kitashima, L.J. Liu, H. Murakami, Numerical analysis of oxygen transport in alpha titanium during isothermal oxidation, J. Electrochem. Soc. 160 (9) (2013) C441–C444, https://doi.org/10.1149/2.100309jes.
[27] T. Kitashima, T. Kawamura, Prediction of oxidation behavior of near-α titanium alloys, Scr. Mater. 124 (2016) 56–58, https://doi.org/10.1016/j.scriptamat.2016.06.044, nov.
[28] C. Ciszak, D. Monceau, C. Desgranges, Modelling the high temperature oxidation of titanium alloys: development of a new numerical tool PyTiOx, Corros. Sci. (2020) 109005, https://doi.org/10.1016/j.corsci.2020.109005, sept.
[29] J. Crank, The Mathematics of Diffusion, 2d ed, Clarendon Press, Oxford, 1975.
[30] T.A. Parthasarathy, W.J. Porter, S. Boone, R. John, P. Martin, Life prediction under tension of titanium alloys that develop an oxygenated brittle case during use, Scr. Mater. 65 (5) (2011) 420–423, https://doi.org/10.1016/j.scriptamat.2011.05.025.
[31] M. Yan, W. Xu, M.S. Dargusch, H.P. Tang, M. Brandt, M. Qian, Review of effect of oxygen on room temperature ductility of titanium and titanium alloys, Powder Metall. 57 (4) (2014) 251–257, https://doi.org/10.1179/1743290114Y.0000000108.
[32] S. Frangini, A. Mignone, F. De Riccardis, Various aspects of the air oxidation behaviour of a Ti6Al4V alloy at temperatures in the range 600-700°C, J. Mater. Sci. 29 (1994) 714–720.
[33] A. Vande Put, C. Thouron, P. Emile, R. Peraldi, B. Dod, D. Monceau, High temperature oxidation and mechanical behavior of β21s and Ti6242s Ti-bases alloys, Proceedings of the 14th World Conference on Titanium (2019).
[34] C. Ciszak, I. Popa, J.-M. Brossard, D. Monceau, S. Chevalier, NaCl induced corrosion of Ti-6Al-4V alloy at high temperature, Corros. Sci. 110 (2016) 91–104, https://doi.org/10.1016/j.corsci.2016.04.016.
[35] K. Maeda, et al., Experimental and theoretical study of the effect of Si on the oxidative behavior of Ti-6Al-4V alloys, J. Alloys. Compd. 776 (2019) 519–528, https://doi.org/10.1016/j.jallcom.2018.10.291.
[36] J. Baillieux, D. Poquillon, B. Malard, Relationship between the volume of the unit cell of hexagonal-close-packed Ti, hardness and oxygen content after α-case formation in Ti–6Al–2Sn–4Zr–2Mo–0.1Si alloy, J. Appl. Crystallogr. 49 (1) (2016) 175–181, https://doi.org/10.1107/S1600576715022906.
[37] David E.A. Garcia, Etude de la diffusion de l'oxygène dans le titane alpha oxydé entre 700 °C et 950 °C, J. Common Met. 65 (1979) 51–69.
[38] A. Casadebaigt, J. Hugues, D. Monceau, Influence of microstructure and surface roughness on oxidation kinetics at 500–600 °C of Ti–6Al–4V alloy fabricated by additive manufacturing, Oxid. Met. 90 (5–6) (2018) 633–648, https://doi.org/10.1007/s11085-018-9859-0.
[39] TITANIUM USA, Executive Summary, 03, Consulté le, juin, 2018, p. 2020 [En ligne]. Disponible sur: https://cdn.ymaws.com/titanium.org/resource/resmgr/02_jens_folder/titanium_usa_2018_executive_.pdf.
[40] D. Poquillon, C. Armand, J. Huez, Oxidation and oxygen diffusion in Ti–6al–4V alloy: improving measurements during sims analysis by rotating the sample, Oxid. Met. 79 (3–4) (2013) 249–259, https://doi.org/10.1007/s11085-013-9360-8.
[41] P. Platt, V. Allen, M. Fenwick, M. Gass, M. Preuss, Observation of the effect of surface roughness on the oxidation of Zircaloy-4, Corros. Sci. 98 (2015) 1–5, https://doi.org/10.1016/j.corsci.2015.05.013, sept.
[42] Z. Liu, G. Welsch, Literature survey on diffusivities of oxygen, aluminum, and vanadium in alpha titanium, beta titanium, and in rutile, Metall. Trans. A 19 (4) (1988) 1121–1125, https://doi.org/10.1007/BF02628396.
[43] P. Kofstad, P.B. Anderson, O.J. Krudtaa, Oxidation of titanium in the temperature range 800-1200°C, J. Common Met. 3 (1961) 89–97.
[44] L. Bataillou, C. Desgranges, L. Martinelli, D. Monceau, Modelling of the effect of grain boundary diffusion on the oxidation of Ni-Cr alloys at high temperature, Corros. Sci. 136 (2018) 148–160, https://doi.org/10.1016/j.corsci.2018.03.001, mai.
[45] D.J. Young, High Temperature Oxidation and Corrosion of Metals, 2nd edition, Elsevier, Amsterdam Boston Heidelberg London, 2016.
[46] G.R. Wallwork, A.E. Jenkins, Oxidation of titanium, zirconium, and hafnium, J. Electrochem. Soc. 106 (1) (1959) 10, https://doi.org/10.1149/1.2427248.
[47] C. Wagner, Theoretical analysis of the diffusion processes determining the oxidation rate of alloys, J. Electrochem. Soc. 99 (10) (1952) 369, https://doi.org/10.1149/1.2779605.
[48] S. Winitzki, A Handy Approximation for the Error Function and Its Inverse, 2008 (consulté le mai 01, 2019), https://www.academia.edu/9730974/A_handy_approximation_for_the_error_function_and_its_inverse.